Multiphoton Laser Microscopy and Fluorescence Lifetime Imaging for the Assessment of the Skin

9

Stefania Seidenari

Abbreviations

BCC	Basal cell carcinoma
FLIM	Fluorescence lifetime imaging
MM	Melanoma
MPT	Multiphoton tomography
NADH	Reduced nicotinamide adenine dinucleotide
NADPH	Reduced nicotinamide adenine dinucleotide phosphate
NIR	Near infrared
SHG	Second harmonic generation
UV	Ultraviolet

Multiphoton laser microscopy or tomography (MPT) associated to fluorescence lifetime imaging (FLIM) is one among the very few noninvasive imaging methods enabling an in vivo optical biopsy. Thanks to its spatial resolution similar to that of histopathology at high power magnification (<1 μm lateral, <2 μm axial) [1] and to the possible use of colour coding of the fluorescence decay time [2, 3], this technique enables the morphology of the tissue to be immediately recognizable.

MPT is an optical imaging system that excites fluorescence from the tissue through the simultaneous absorption of two or more photons of infrared light [4]. Whereas for conventional confocal fluorescence microscopy, fluorophores are excited by absorption of individual photons in the visible or ultraviolet spectrum, MPT excitation entails the simultaneous absorption of two or more photons of longer wavelength. This process requires a high intensity of excitation light and is confined to the tightly focused excitation spot. The longer wavelength infrared radiation undergoes less scattering than visible light and can thus facilitate high resolution imaging deeper into biological tissue [1, 4–13].

MPT can exploit autofluorescence of intrinsic tissue fluorophores, i.e. naturally occurring molecules that can be imaged using MPT without the need for exogenous contrast agents. Fluorophores are integral components of the molecules to which they confer the characteristic autofluorescence. They include NADH (reduced nicotinamide adenine dinucleotide), NADPH (reduced nicotinamide adenine dinucleotide phosphate), flavines, keratin, melanin, elastin, collagen, porphyrin, tryptophan, cholecalciferol and lipofuscin [1, 4–13]. After energy absorption, fluorophores can then emit energy in turn, generating a visible signal at defined and characteristic wavelengths, different from those of absorption. The quantity and the wavelength of the emitted energy depend on the chemical characteristics of the fluorophore, on its environment and particularly on the type of the surrounding molecules [14–16].

Efficient MPT excitation usually requires ultrashort femtosecond laser pulses, which are also able to produce the nonlinear effect of second harmonic generation (SHG). The SHG signal comes

S. Seidenari
Department of Dermatology,
University of Modena and Reggio Emilia,
via del Pozzo 71, Modena 41100, Italy
e-mail: stefania.seidenari@skincenter.it,
stefania.seidenari@unimore.it

E. Berardesca et al. (eds.), *Non Invasive Diagnostic Techniques in Clinical Dermatology*,
DOI 10.1007/978-3-642-32109-2_9,

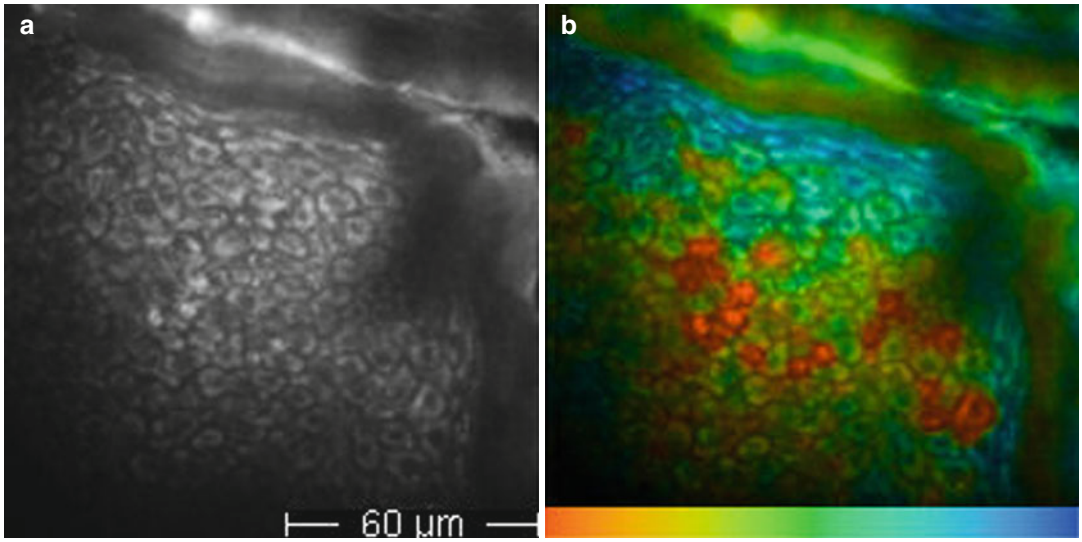

Fig. 9.1 On the *left* (**a**), multiphoton tomography intensity image of healthy epidermis. In (**b**) pseudo-colour-coded fluorescence lifetime image of the same epidermal area, where *red-coloured* melanocytes, characterized by a short lifetime decay time, are well distinguishable from *green-coloured* keratinocytes with a medium lifetime value. Pseudo-colour scale: 0–2,000 ps

from periodic structures such as collagen and is characterized by an emission wavelength corresponding to half of that of the incident photon; this particular signal allows the visualization of dermal collagen bundles and their distinction from cellular components and elastin fibres [1, 5, 6]. With MPT bidimensional images are acquired which correspond to optical sectioning parallel to the tissue surface (reported to a defined xy-plane). Pictures obtained at various depths, called z-stacks, can be acquired by sequentially modifying the depth of the focal plane in the tissue, reaching levels of 200 µm measured from the departure point at the skin surface [8, 10, 13]. Grey scale images are generated, reproducing the fluorescence intensity in different tissue components (Fig. 9.1a).

9.1 Excitation Wavelength

By modulating the excitation wavelength, different skin structures can be selectively excited, obtaining an enhancement of their morphology. When exploring the skin, a wavelength of 760 nm is first chosen for a proper imaging of epidermal structures [8, 10, 13]. When reaching the dermo-epidermal junction, the excitation wavelength has to be increased up to 800–820 nm, for selective melanin imaging. By this wavelength, most keratinocytes progressively become invisible. On the contrary, since melanin has an absorption spectrum that decreases from the UV region to NIR, with a selective excitation wavelength of 800 nm [17–19], melanin and melanin-containing cells (melanocytes and melanin-containing keratinocytes) will appear as single cells in the basal layer showing intense fluorescence. This characteristic can be employed to recognize melanocytes and melanin granules in cell cultures (Fig. 9.2).

A wavelength of 800 nm is generally employed to adequately visualize the extracellular matrix of the dermis. At this wavelength, collagen fibres that generate the SHG signal are selectively excited, whereas at 760 nm, dermal autofluorescent components such as elastin are enhanced in the image.

9.2 Fluorescence Lifetime Imaging

Fluorescence lifetime imaging (FLIM) is based on the measurement of the decay rate of the fluorescence signal following a short pulse of

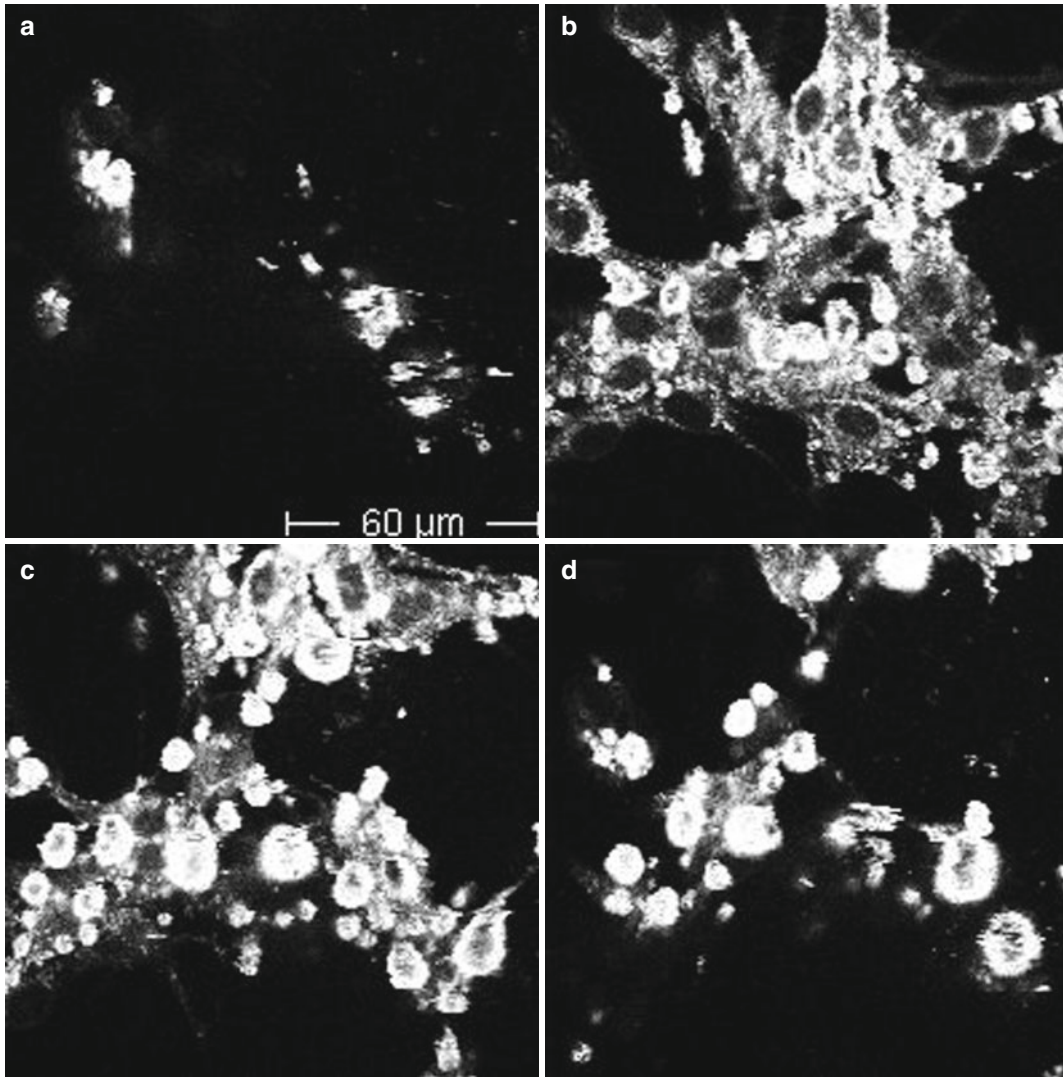

Fig. 9.2 Multiphoton tomography intensity images. Melanin imaging and excitation wavelength. In a melanocyte cell culture, by a 720-nm excitation wavelength (**a**), cells and melanin granules are not recognizable; (**b**) at 760 nm, both melanocytes and melanin granules are clearly visible; (**c**, **d**) by increasing the excitation wavelength to 780 and 800 nm, melanin granules are enhanced, but melanocyte bodies fade (**c**) and are not more visible (**d**)

excitation light [11, 15, 19]. This represents an additional technique for use in combination with MPT (MPT/FLIM), further improving the understanding of skin morphology in detail. Further discrimination between fluorophores can be gained using multispectral FLIM, which is based on the analysis of multiple emission spectral channels [20–22].

Whereas MPT conventionally relies on the assessment of the intensity of endogenous fluorescence emitted by fluorophores in the skin, FLIM provides additional information based on the contrast generated by differences in the decay rate of the fluorescence intensity, not only providing morphological information but also a quantitative assessment of metabolic changes in living tissue. Since FLIM is immune to intensity artefacts, it enables a more robust numerical description of the images than intensity imaging [2, 20–22]. Images presented in this chapter are obtained by a FLIM system, developed jointly by the Photonics Group of the Imperial College of London and

JenLab GmbH (Jena, Germany), which has been incorporated into the commercially available *DermaInspect®* (JenLab GmbH, Jena, Germany). The distribution of fluorescence lifetimes within an image is visualized through a histogram that plots the fluorescence lifetime (*x*-axis) against the number of corresponding pixels occurring at that lifetime (*y*-axis). Pseudo-colour images are generated, where each image pixel contains information about its fluorescence decay time corresponding to a specific colour. Thus, four dimensional data sets are generated, where the tissue is not only studied according to its structure in the *x*-, *y*- or *z*-axis but also according to the fluorescence dynamics of its components corresponding to different states or metabolic characteristics of the tissue [2, 20–22]. Besides essential information on fluorescence decay rates, false colour coding, enhancing image contrast and providing a more user-friendly visualization method permits the immediate identification of cellular, subcellular or extracellular structures in the image. As an example, when employing a 0–2,000 scale, keratinocytes, exhibiting fluorescence decay time values around 1,000 ps, are represented in the blue-green range, whereas melanocytes, with medium to short fluorescence decay time, are coded in the yellow-red range (Fig. 9.1b) [23]. Fluorescence lifetime scale intervals may be varied according to the need for enhancing particular structures or cells belonging to a certain typology or to identify subcellular particles. Figure 9.3 shows upper melanoma layers represented by two different scales. On the left, employing a 0–2,000 colour scale, melanoma cells are coloured red, corresponding to short-lifetime values, and this permits the immediate categorization into melanin-containing cells; on the right, short-lifetime values are expanded employing a 0–400 scale, enabling the enhancement of intracellular structures.

9.3 Application Fields

Cell Cultures. The MPT/FLIM technique has numerous applications in dermatology. Morphologic and metabolic characteristics of different cell types can be studied employing cell cultures,

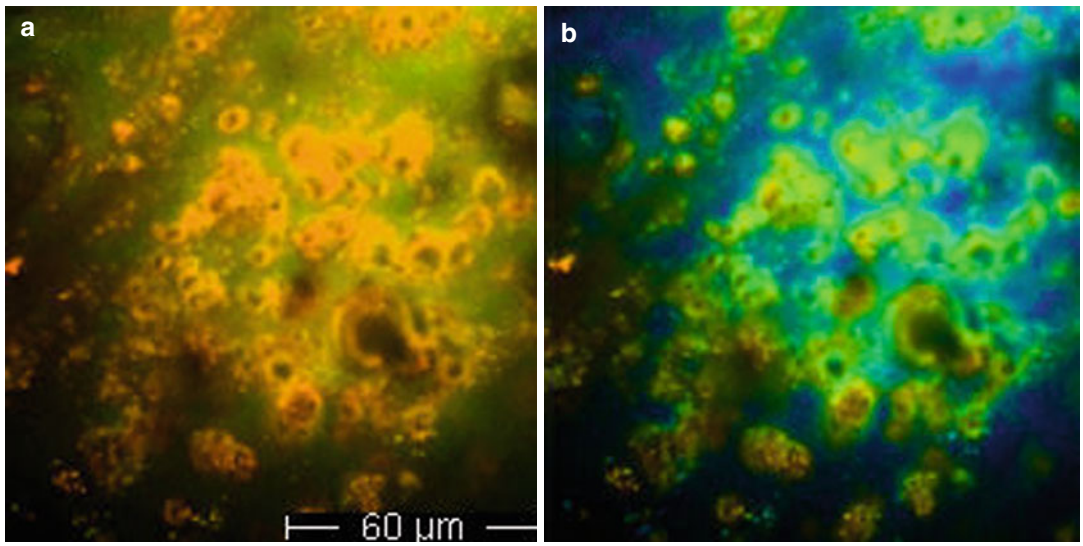

Fig. 9.3 On the *left* (**a**), *upper* melanoma layers represented by a 0–2,000 ps pseudo-colour scale. Melanoma cells, displaying short lifetime values, are shown in *orange* and are immediately recognizable. On the *right* (**b**), a 0–400 ps scale is employed to increase the contrast inside cell components and to recognize the characteristics of the cytoplasm. Images presented in this chapter were obtained by a FLIM system, developed jointly by the Photonics Group of the Imperial College of London and JenLab GmbH (Jena, Germany), which has been incorporated into the commercially available *DermaInspect®* (JenLab GmbH, Jena, Germany) and were calculated using the software SPCImage (Becker & Hickl GmbH)

where isolated cells can be examined out of the tissue environment. Fibroblast cultures are widely used as an experimental model to study the expression of specific genes or the effect of drugs with potential chemotherapeutic activity and to check the mutagenicity and carcinogenicity of different substances. Using MPT/FLIM, a precise and rapid assessment of the morphologic and metabolic changes fibroblasts undergo after exposure to various environmental factors can be achieved without the need of cell processing and staining [24] (Fig. 9.4).

Healthy Skin and Skin Ageing. Healthy epidermis shows a homogenous distribution of cells which are divided by thin nonfluorescent intercellular spaces [7–13, 23, 25]. Since nuclei are deficient in autofluorescence signals, they appear as dark areas inside the fluorescent cytoplasm (Figs. 9.1a and 9.5). The stratum corneum shows strong keratin-based fluorescent hexagonal-shaped large flat cells. At a depth of about 20 μ from the skin surface, we find the stratum granulosum, where keratinocytes appear as large, oval cells with autofluorescence in the cytoplasm and dark nuclei. Melanin blotches inside the keratinocytes may be unique, involving a large part of the cytoplasm and sparing the nucleus, or may be organized in multiple spots, conferring a granular appearance to the keratinocyte. Sometimes the melanin blotch forms a cap over the nucleus, which is not recognizable because of the horizontal optical section of the sample. Stratum spinosum cell diameter decreases and cell density increases going more in depth towards the basal layer. At 50–100 μ from the skin surface, we find the basal layer with brightly fluorescent small polygonal keratinocytes and dark nuclei. At the dermo-epidermal junction, we find dark round/oval-shaped areas, interrupting the basal layer, corresponding to the top of the dermal papillae, where we can appreciate the presence of fibres [23].

The morphology and the metabolic states of healthy skin can be assessed in vivo, according to skin site and age. In fact, cell diameter and density vary according to epidermal cell depth and skin site [23]. In the elderly, epidermal cells show morphologic alterations, presenting irregular shape, size and intercellular distance and a decreased number at the basal layer (Fig. 9.5d). The modifications of the metabolic activities characteristic of the ageing process are reflected by variations in FLIM values, which increase at both the upper and lower layers in elderly subjects [23]. Further efforts are needed to increase knowledge on variations the epidermis undergoes according to environmental influences, for use as

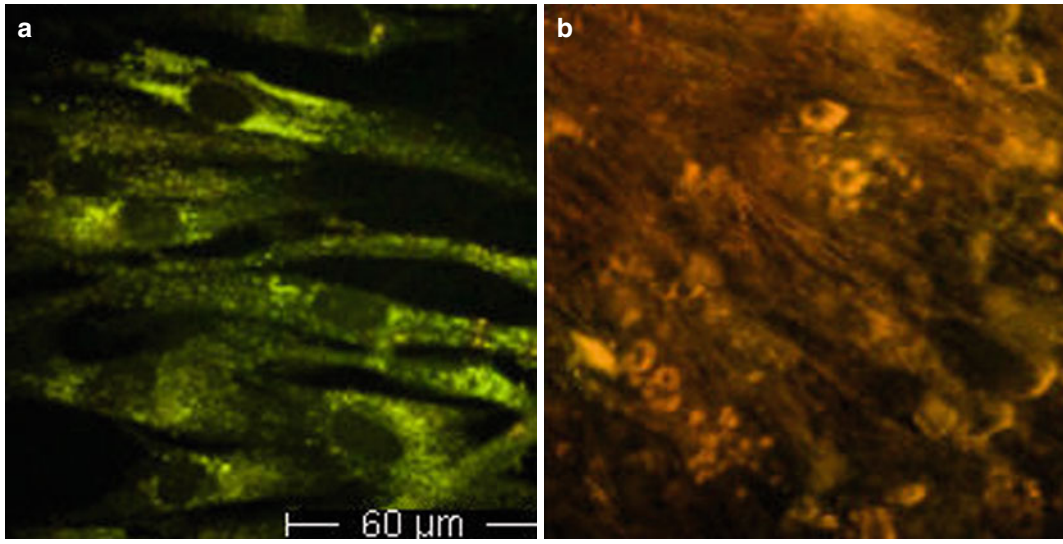

Fig. 9.4 On the *left* (**a**), a 3-day old fibroblast culture; on the *right* (**b**), a 1 month old culture stimulated with ascorbic acid where the fibres produced by the fibroblast are clearly visible as *red* (short-lifetime) filaments

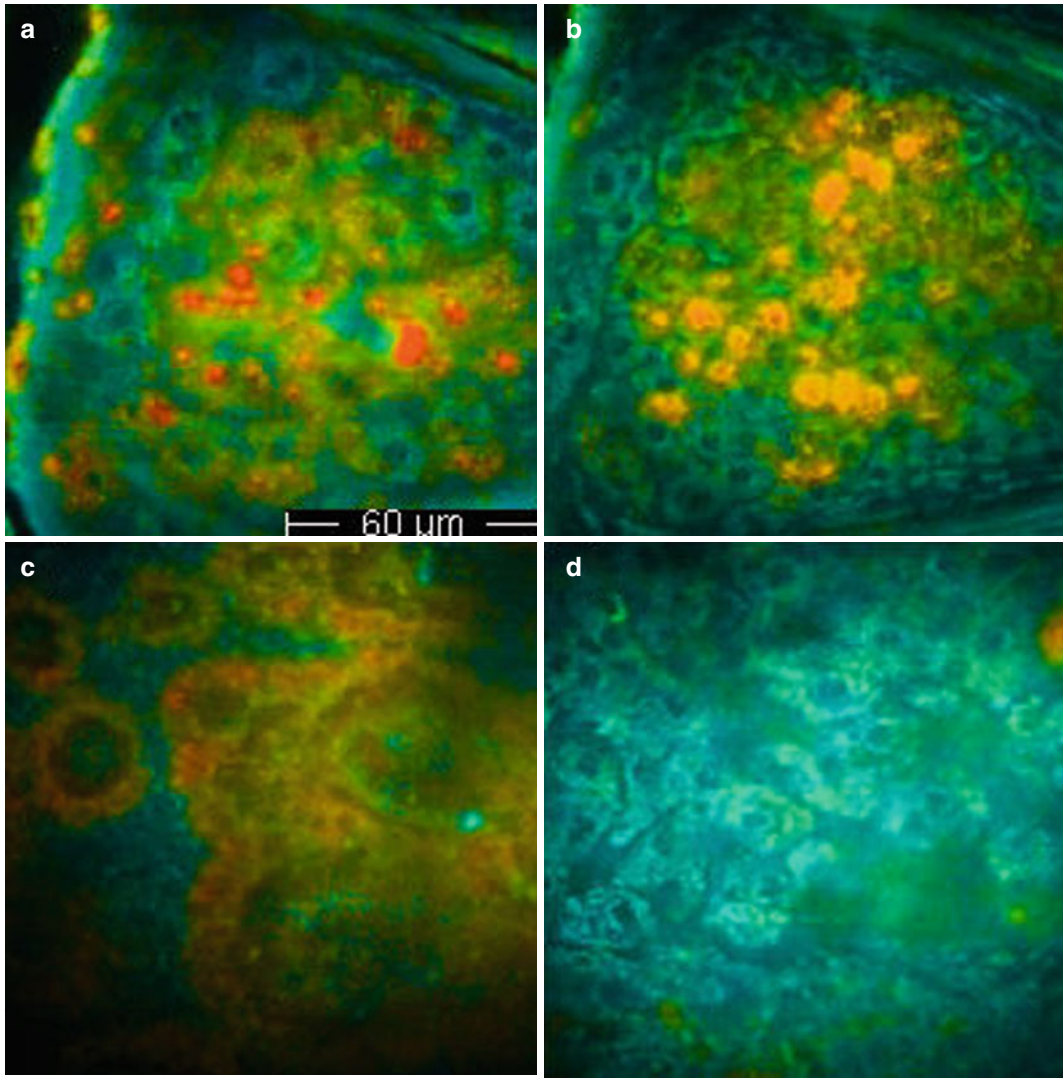

Fig. 9.5 (**a**–**c**) Pseudo-colour FLIM stack of healthy epidermis. (**a**) *Upper* epidermal layers of a young subject, (**b**) *lower* epidermal layers, (**c**) dermo-epidermal junction and (**d**) *upper* epidermal layers in an elderly subject. In (**a**), keratinocytes show regular contours and intercellular distance, whereas in (**d**) cells present morphologic alterations and a shift of the fluorescence decay time towards higher values (*blue-coloured keratinocytes*)

the SHG component of the signal when exciting at up to 800–820 nm. When employing the filter eliminating the SHG signal, collagen fibres only contribute to the signal with their modest autofluorescence component, thus fading and enabling the recognition of fibres containing elastin. The latter appear as fine-curled fibres with a nonhomogeneous calibre (Fig. 9.6).

Skin ageing and pathological skin conditions of the dermis bring about morphological changes in the dermal collagen and elastin fibre network. papillary dermis. Conversely, in the elderly, SHG signals can only be detected in the uppermost part of the dermis, whereas large amounts of fluorescent elastic fibres, corresponding to solar elastosis, are found in the dermis [28]. The trend of decreasing SHG signals and increasing autofluorescence signals is correlated with the histological findings of the decrease in collagen fibres and the increase in elastic fibres with increasing age.

MPT/FLIM is a procedure holding great promise for increasing diagnostic accuracy of skin tumours.

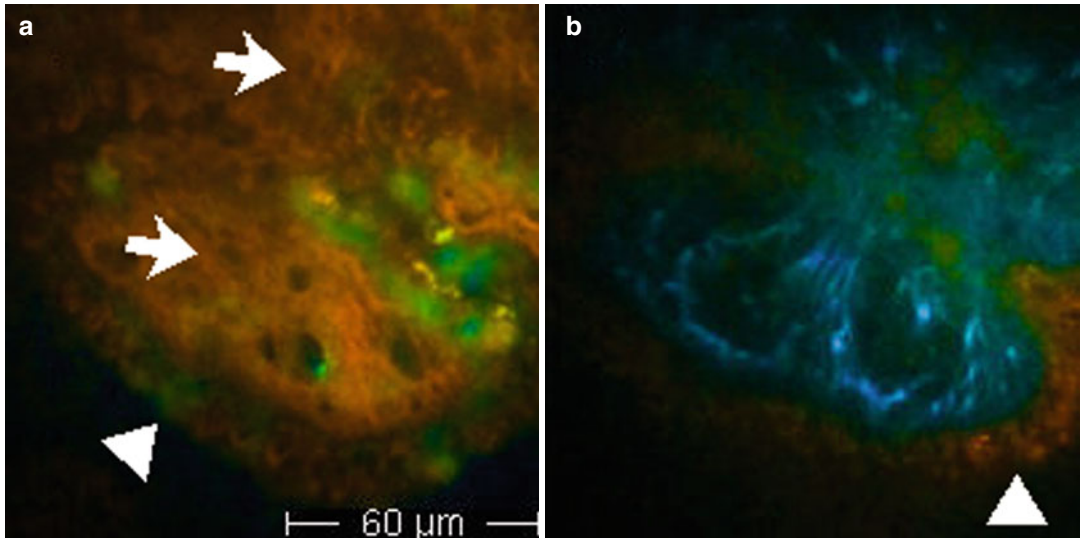

Fig. 9.6 MPT/FLIM: pseudo-colour-coded fluorescence lifetime imaging (pseudo-colour scale 0–2,000 ps). Enhancement of elastin fibres by inserting a filter for SHG signals originating from collagen fibres. A nevus at a depth of –60 **µ**. (**a**) Collagen fibres (*white arrows*) appear as thick *red* filaments inside the dermal papillae; (**b**) after filtering SHG signals, elastin fibres appear as tiny blue (long-lifetime) filaments; melanocytes surround the papillae (*triangle*)

Basal Cell Carcinoma (BCC). BCC represents the most frequent skin tumour. Besides the diagnostic difficulties for superficial lesions which lack sensitive dermoscopic criteria, the identification of tumour boundaries, and consequently of the excision margins, represents practical problems in the daily dermatological routine. The use of MPT alone has already proved effective in identifying some diagnostic aspects of BCC. Investigating BCC specimens by MPT, histopathological features characteristic of BCC, such as elongated cells, nuclei polarization and peripheral palisading, can be recognized in the images [29, 30]. Lin et al. achieved a discrimination of BCC from normal dermal stroma by MPT imaging of formalin-fixed specimens of nine nodular type BCCs [31]. BCCs appeared as clumps of autofluorescent cells with large nuclei and peripheral palisading. By FLIM implementation and valuable information about time-resolved analysis of the fluorescence signal, further criteria are added for diagnostic purposes and tumour margin assessment. Using a multidimensional nonlinear laser imaging approach to visualize *ex vivo* samples of BCC, Cicchi et al. observed a blue-shifted fluorescence emission, a higher fluorescence response at 800 nm excitation wavelength and a slightly longer mean fluorescence lifetime in BCCs [32]. A wide-field (single photon excitation) study by Galletly et al. employing FLIM, imaged unstained excision biopsies of 25 BCCs with FLIM following excitation of autofluorescence with a 355 nm pulsed ultraviolet laser [3]. A significant reduction in mean fluorescence lifetimes between areas of BCC and those of surrounding uninvolved skin was demonstrated. Investigating BCC by MPT, Seidenari et al. identified specific descriptors, which were never observed in healthy skin but were present in all BCCs [30]. Further examination of BCC by MPT/FLIM revealed that some of these features correspond to traditional histopathological diagnostic criteria, such as aligned elongated monomorphous cells, peripheral palisading of tumour cells and typical tumour nests, whereas others, such as ‘blue cells’ and ‘phantom islands’, cannot be recognized in fixed and stained specimens (Fig. 9.7) [33]. ‘Blue cells’ correspond to basaloid cells showing fluorescence lifetime values higher than those of normal keratinocytes. The biological significance of the lifetime modifications in cancer cells is thought to be due to a shift from oxidative metabolism to

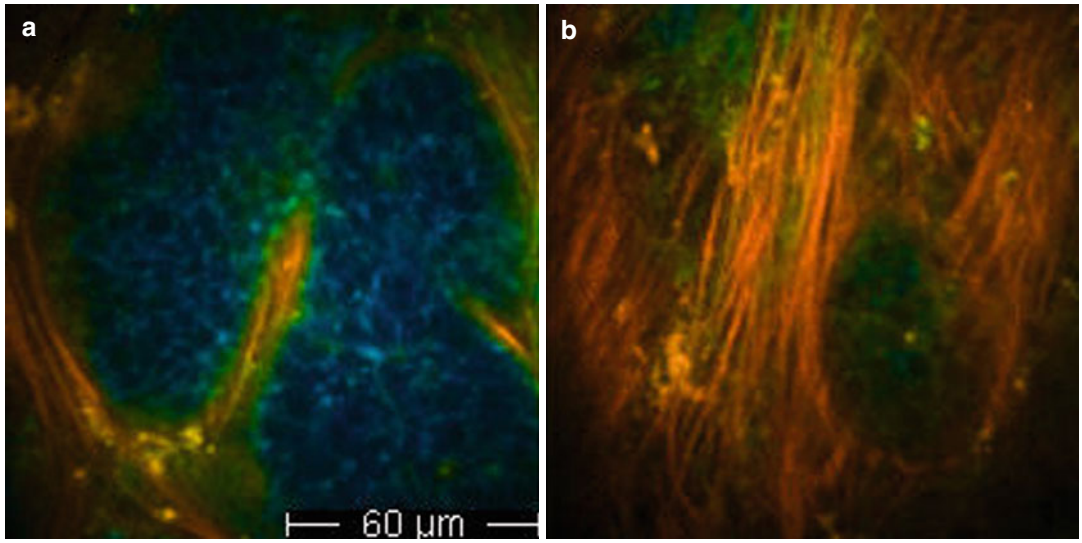

Fig. 9.7 On the *left* (**a**), basal cell carcinoma nests constituted by '*blue cells*'; on the *right* (**b**), 'phantom islands', i.e. basal cell carcinoma nests disappearing at an excitation wavelength of 800 nm; at the same time, collagen fibres are enhanced and appear as *red* filaments circumscribing the nests

glycolysis associated to variations in the amount of free and bound NADH [14]. Thus, FLIM imaging may represent a method to measure the oxidative stress and/or preferential metabolic pathway in living tissues [14]. 'Phantom islands' are generated by shifting the excitation wavelength to 800–820 nm. In this way, keratinocytes and BCC cells almost disappear, whereas the visualization of fibres is enhanced. Short-lifetime red (collagen) fibres tightly embrace the basaloid longer lifetime blue cell nests, corresponding to empty spaces ('phantom islands') (Fig. 9.7). Employing the MPT/FLIM technique, the separation between healthy skin and the tumour mass is achieved in all cases, making this technique a consistent tool for the definition of tumour margins.

Melanocytic Nevi. Common nevi, which are characterized by a proliferation of typical melanocytes, in single cells or in aggregates, are benign lesions which are clinically relevant as their appearance may be very similar to malignant melanocytic lesions. By MPT/FLIM, specific descriptors, referring both to cytology and architecture, enable their diagnosis [34]. Melanin-containing keratinocytes are recognizable in FLIM images as long-lifetime cells containing short-lifetime spots or blotches (red to yellow in the 0–2,000 ps pseudo-colour scale) characterizing melanin, whereas epidermal melanocytes in the upper and the lower layers appear as tiny short-lifetime cells, which are smaller than keratinocytes presenting a well visible small nucleus and homogeneously distributed melanin (Fig. 9.8a). At the dermo-epidermal junction level, the tips of the dermal papillae, appearing as roundish structures surrounded by a regular orange boundary of melanin-containing keratinocytes and melanocytes, are visible. 'Edged papillae' are characterized by a well-demarcated rim of orange cells surrounding a dark space containing fibres or cells, whereas 'non-edged papillae' lack a well-defined boundary (Fig. 9.9). Junctional nevus cell nests appear as aggregates of short-lifetime cells rising from the periphery of the papillae (Fig. 9.9). In compound nevi, short-lifetime 'dermal cell clusters' are also visible (Fig. 9.8b). By MPT/FLIM a regular architecture is generally observable in benign melanocytic lesions.

Melanoma. Melanoma (MM) is a lethal cancer. Despite a high cure rate for thin melanomas, advanced melanomas have a poor prognosis. Thus, early identification of melanoma represents a crucial end point for physicians. Due to its high resolution, MPT/FLIM holds a great potential for improving MM diagnosis [19, 35].

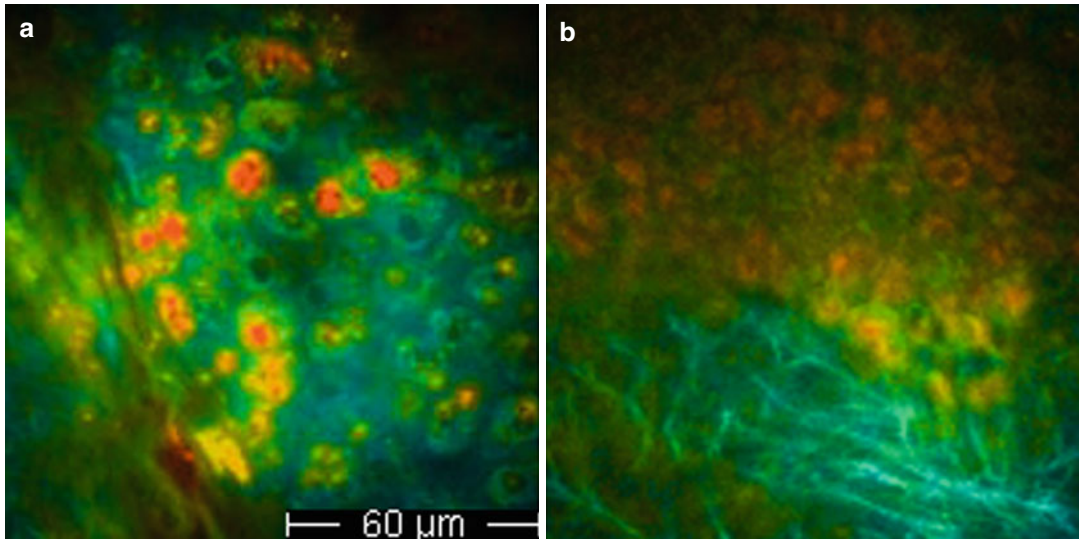

Fig. 9.8 On the *left* (**a**), pseudo-colour-coded fluorescence lifetime image of *upper layers* in a nevus, where *small red-coloured* melanocytes, characterized by a short-lifetime decay time, are well distinguishable from *large green-coloured* keratinocytes with a medium lifetime value. The pseudo-colour scale employed to represent this picture ranges from 500 to 2,000 ps. On the *right* (**b**), a dermal melanocyte cluster in a compound nevus; *blue* elastin fibres are visible in the dermis

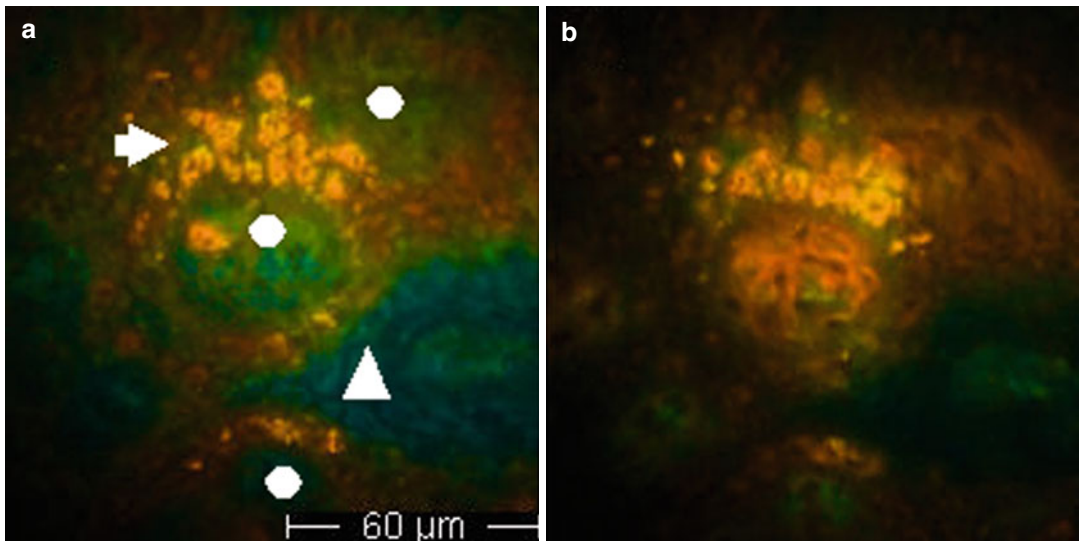

Fig. 9.9 Selective melanin imaging and enhancement of collagen fibres by switching the excitation wavelength from 760 (**a**) to 800 nm (**b**). A nevus at a depth –60 m. Pseudo-colour scale: 0–2,100 ps. (**a**) By a 760-nm excitation wavelength, dermal papillae (*white dots*) are surrounded by *red* short-lifetime cells (melanin-containing cells), forming a junctional nest (*arrow*), whereas keratinocytes (*white triangle*) appear *green*. (**b**) By an excitation wavelength of 800 nm, melanin-containing cells maintain their visibility, whereas keratinocytes disappear. Inside the papillae, collagen fibres appear as *thick red* (short-lifetime) filaments

By MPT/FLIM, keratinocytes may not be recognizable at the superficial layers of a MM. When present, they are infiltrated by atypical melanocytes [36]. When displaying images by a 0–2,000 ps fluorescence lifetime range, MM cells appear orange to red, due to their short

fluorescence decay time, and this immediately enables the determination of the melanocytic nature of the lesion (Fig. 9.3a). To increase contrast for the distinction of image details, a 0–400 scale is then applied (Fig. 9.3b). At the superficial level, atypical MM cells appear as large short-lifetime cells with a nucleus with undefined contours and a nonhomogeneous cytoplasm with speckled melanin. A peripheral cytoplasmic halo is often observable due to variable lifetime values of different cell areas (Fig. 9.3). Deeper MM layers show atypical short-lifetime cells smaller in size with respect to those observable on the surface; these are pleomorphic, variable in size and irregular in shape with a nonhomogeneous distribution. At this level, atypical short-lifetime cells may form aggregates or nests and may infiltrate dermal papillae and hair follicles. When dermal papillae are recognizable, these are not usually surrounded by a rim of regularly arranged melanocytes; they are irregularly sized and shaped and are separated by interpapillary spaces of different thickness. An architectural disorder is always visible. In MM metastases, besides atypical short-lifetime cells, long-lifetime (lacking melanin) cell nests are intermingled with long-lifetime (collagen) fibres (Fig. 9.10).

9.4 Advantages, Disadvantages and Future Objectives of MPT/FLIM

The morphology of MPT/FLIM images, acquired with a spatial resolution similar to that of histopathology at high power magnification, is extremely coherent with that of the histopathological analysis, suggesting that this new technique, once fully developed, may replace histology [1, 10].

Intensity images are visualized during the examination process in real time. FLIM images require a further elaboration to allow the operational system to develop a diagram of the fluorescence decay time and to produce a pseudo-colour image [3, 22]. Not only does MPT/FLIM generate high resolution images providing highly informative morphologic details but it also enables the study of the kinetics of the fluorescence decline and the calculation of the mean fluorescence intensity and lifetime values for selected areas of interest such as the cytoplasm of single cells, providing numerical data for an objective assessment of physiologic and pathologic skin conditions [2–4, 22]. The subcellular spatial resolution study of tissue samples in three dimensions is made possible by the acquisition of a sequence of horizontal optical sections (stack).

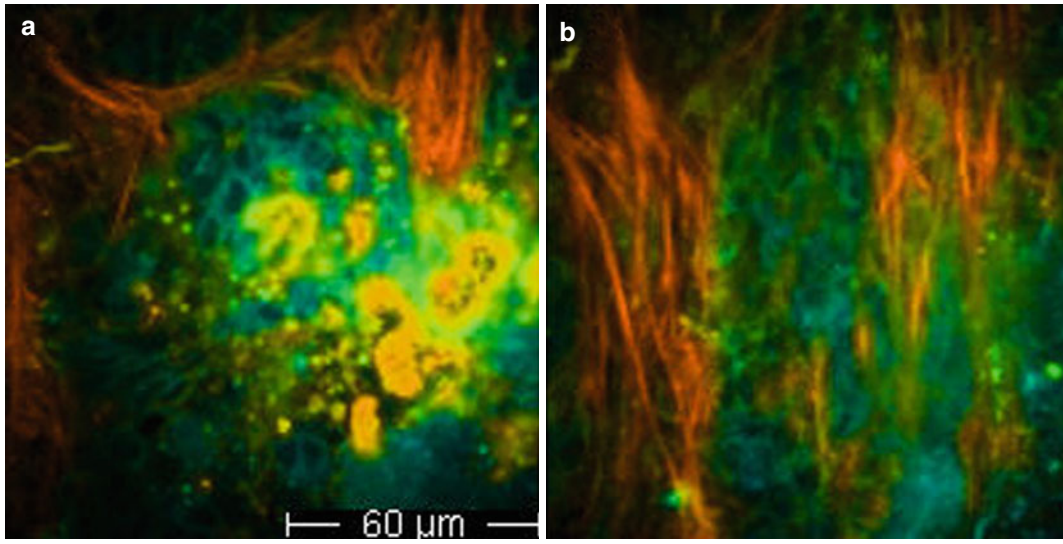

Fig. 9.10 Melanoma metastases. On the *left* (**a**), atypical melanocytes (*orange* short-lifetime cells) and collagen fibres; on the *right* (**b**), nests of atypical long-lifetime cells (atypical melanocytes not producing melanin) intermingled with fibres

Moreover, the nonlinear excitation produced by the NIR radiation allows a higher visualization of the deep dermis. The potential of this technique to provide an improvement in diagnostic accuracy is especially valuable for skin tumours, where an 'optical biopsy' enabling a diagnosis on the basis of both architectural and cellular morphology and numerical parameters is immediately available.

Long-term studies of cutaneous affections can be performed by the repetition of the in vivo examination on the same explored skin site within short or long intervals, considering that this technique has proved noninvasive [9].

On the other hand, the MPT/FLIM technique is at present unsuitable for continuous clinical use, since it presents some drawbacks consisting in a long acquisition/elaboration time of the images and the small field of view. Thus, important goals are both to reduce the acquisition time to avoid imaging deformities caused by voluntary and involuntary movements and to implement a device enabling the imaging of skin areas, large enough to be representative of the entire lesion.

References

1. König K, Riemann I (2003) High-resolution multiphoton tomography of human skin with subcellular spatial resolution and picoseconds time resolution. J Biomed Opt 8(3):432–439
2. Elson D, Requejo-Isidro J, Munro I, Reavell F, Siegel J, Suhling K, Tadrous P, Benninger R, Lanigan P, McGinty J, Talbot C, Treanor B, Webb S, Sandison A, Wallace A, Davis D, Lever J, Neil M, Phillips D, Stamp G, French P (2004) Time-domain fluorescence lifetime imaging applied to biological tissue. Photochem Photobiol Sci 3:795–801
3. Galletly NP, McGinty J, Dunsby C, Teixeira F, Requejo-Isidro J, Munro I, Elson DS, Neil MA, Chu AC, French PM, Stamp GW (2008) Fluorescence lifetime imaging distinguishes basal cell carcinoma from surrounding uninvolved skin. Brit J Dermatol 159:152–161
4. Denk W, Strickler JH, Webb WW (1990) Two-photon laser scanning fluorescence microscopy. Science 248:73–76
5. Kollias N, Zonios G, Stamatas GN (2002) Fluorescence spectroscopy of skin. Vib Spectrosc 28(1):17–23
6. Zipfel WR, Williams RM, Christie R, Nikitin AY, Hyman BT, Webb WW (2003) Live tissue intrinsic emission microscopy using multiphoton-excited native fluorescence and second harmonic generation. Proc Natl Acad Sci U S A 100(12):7075–7080
7. Riemann I, Dimitrow E, Fischer P, Reif A, Kaatz M, Elsner P, König K (2004) High resolution multiphoton tomography of human skin in vivo and in vitro. SPIE-Proc 21–28
8. Schenke-Layland K, Riemann I, Damour O, Stock UA, König K (2006) Two-photon microscopes and in vivo multiphoton tomographs-powerful diagnostic tools for tissue engineering and drug delivery. Adv Drug Deliv Rev 58(7):878–896
9. Lin SJ, Jee SH, Dong CY (2007) Multiphoton microscopy: a new paradigm in dermatological imaging. Eur J Dermatol 17(5):361–366
10. König K (2008) Clinical multiphoton tomography. Review. J Biophotonics 1(1):13–23
11. Cicchi R, Sestini S, De Giorgi V, Massi D, Lotti T, Pavone FS (2008) Nonlinear laser imaging of skin lesions. J Biophotonics 1(1):62–73
12. Tsai TH, Jee SH, Dong CY, Lin SJ (2009) Multiphoton microscopy in dermatological imaging. J Dermatol Sci 56(1):1–8
13. König K, Raphael AP, Lin L, Grice JE, Soyer HP, Breunig HG, Roberts MS, Prow TW (2011) Applications of multiphoton tomographs and femtosecond laser nanoprocessing microscopes in drug delivery research. Adv Drug Deliv Rev 63(4–5):388–404
14. Skala MC, Riching KM, Gendron-Fitzpatrick A, Eickhoff J, Eliceiri KW, White JG, Ramanujam N (2007) In vivo multiphoton microscopy of NADH and FAD redox states, fluorescence lifetimes, and cellular morphology in precancerous epithelia. Proc Natl Acad Sci U S A 104(49):19494–19499
15. Sanchez WY, Prow TW, Sanchez WH, Grice JE, Roberts MS (2010) Analysis of the metabolic deterioration of ex vivo skin from ischemic necrosis through the imaging of intracellular NAD(P)H by multiphoton tomography and fluorescence lifetime imaging microscopy. J Biomed Opt 4:046008
16. Palero JA, Bader AN, de Bruijn HS, Der Ploeg van den Heuvel A, Sterenborg HJ, Gerritsen HC (2011) In vivo monitoring of protein-bound and free NADH during ischemia by nonlinear spectral imaging microscopy. Biomed Opt Express 2(5):1030–1039
17. Teuchner K, Freyer W, Leupold D, Volkmer A, Birch DJ, Altmeyer P, Stücker M, Hoffmann K (1999) Femtosecond two-photon excited fluorescence of melanin. Photochem Photobiol 70(2):146–151
18. Teuchner K, Ehlert J, Freyer W et al (2000) Fluorescence studies of melanin by stepwise two-photon femtosecond laser excitation. J Fluoresc 10:275–281
19. Dimitrow E, Riemann I, Ehlers A, Koehler MJ, Norgauer J, Elsner P, König K, Kaatz M (2009) Spectral fluorescence lifetime detection and selective melanin imaging by multiphoton laser tomography for melanoma diagnosis. Exp Dermatol 18(6): 509–515
20. Becker W, Bergmann A, Biskup C (2007) Multispectral fluorescence lifetime imaging by TCSPC. Microsc Res Tech 70(5):403–409
21. Talbot CB, Patalay R, Munro I, Warren S, Ratto F, Matteini P, Pini R, Breunig HG, König K, Chu AC,

Stamp GW, Neil MA, French PM, Dunsby C (2011) Application of ultrafast gold luminescence to measuring the instrument response function for multispectral multiphoton fluorescence lifetime imaging. Opt Express 19(15):13848–13861
22. Patalay R, Talbot C, Alexandrov Y, Munro I, Neil MA, König K, French PM, Chu A, Stamp GW, Dunsby C (2011) Quantification of cellular autofluorescence of human skin using multiphoton tomography and fluorescence lifetime imaging in two spectral detection channels. Biomed Opt Express 2(12):3295–3308, Epub 2011 Nov 10
23. Benati E, Bellini V, Borsari S, Dunsby C, Ferrari C, French P, Guanti M, Guardoli D, Koenig K, Pellacani G, Ponti G, Schianchi S, Talbot C, Seidenari S (2011) Quantitative evaluation of healthy epidermis by means of multiphoton microscopy and FLIM. Skin Res Technol 17:295–303
24. Rice WL, Kaplan DL, Georgakoudi I (2010) Two-photon microscopy for non-invasive, quantitative monitoring of stem cell differentiation. PLoS One 5(4):e10075
25. Seidenari S, Arginelli F, Bassoli S, Cautela J, French P, Guanti M, Guardoli D, König K, Talbot C, Dunsby C (2012) Multiphoton laser microscopy and fluorescence lifetime imaging for the evaluation of the skin. Dermatol Res Pract 2012:810749
26. Koehler MJ, Preller A, Kindler N, Elsner P, König K, Bückle R, Kaatz M (2003) Intrinsic, solar and sunbed-induced skin aging measured in vivo by multiphoton laser tomography and biophysical methods. Skin Res Technol 15(3):357–363
27. Koehler MJ, Hahn S, Preller A, Elsner P, Ziemer M, Bauer A, König K, Bückle R, Fluhr JW, Kaatz M (2008) Morphological skin ageing criteria by multiphoton laser scanning tomography: non-invasive in vivo scoring of the dermal fibre network. Exp Dermatol 17(6):519–523
28. Lin SJ, Wu R Jr, Tan HY, Lo W, Lin WC, Young TH, Hsu CJ, Chen JS, Jee SH, Dong CY (2005) Evaluating cutaneous photoaging by use of multiphoton fluorescence and second-harmonic generation microscopy. Opt Lett 30(17):2275–2277
29. Paoli J, Smedh M, Wennberg AM, Ericson MB (2008) Multiphoton laser scanning microscopy on non-melanoma skin cancer: morphologic features for future non-invasive diagnostics. J Invest Dermatol 128(5): 1248–1255
30. Seidenari S, Arginelli F, Bassoli S, Cautela J, Cesinaro AM, Guanti M, Guardoli D, Magnoni C, Manfredini M, Ponti G, König K (2013) Diagnosis of BCC by multiphoton laser tomography. Skin Res Technol 19(1):e297–e304
31. Lin SJ, Jee SH, Kuo CJ, Wu RJ, Lin WC, Chen JS, Liao YH, Hsu CJ, Tsai TF, Chen YF, Dong CY (2006) Discrimination of basal cell carcinoma from normal dermal stroma by quantitative multiphoton imaging. Opt Lett 31(18):2756–2758
32. Cicchi R, Massi D, Sestini S, Carli P, De Giorgi V, Lotti T, Pavone FS (2007) Multidimensional non-linear laser imaging of basal cell carcinoma. Opt Express 15(16): 10135–10148
33. Seidenari S, Arginelli F, French P, König K, Magnoni C, Manfredini M, Ponti G, Talbot C, Dunsby C (2012) Multiphoton laser tomography and fluorescence lifetime imaging of basal cell carcinoma: morphologic features for non-invasive diagnostics. Exp Dermatol 21(11):831–836
34. Arginelli F, Manfredini M, Bassoli M, Dunsby C, French P, König K, Magnoni C, Ponti G, Talbot C, Seidenari S (2013) High resolution diagnosis of common nevi by multiphoton laser tomography and fluorescence lifetime imaging. Skin Res Technol 19(2):194–204
35. Dimitrow E, Ziemer M, Koehler MJ, Norgauer J, König K, Elsner P, Kaatz M (2009) Sensitivity and specificity of multiphoton laser tomography for in vivo and ex vivo diagnosis of malignant melanoma. J Invest Dermatol 129(7):1752–1758
36. Seidenari S, Arginelli F, Bassoli M, Dunsby C, French P, König K, Magnoni C, Ponti G, Talbot C. Multiphoton laser tomography and fluorescence lifetime imaging improve the diagnostic accuracy of melanoma. Submitted (in press)